Proceedings of the 5th International Conference on Civil Engineering Fundamentals and Applications (ICCEFA 2024)
Lisbon, Portugal- November 18 - 20, 2024
Paper No. 142
DOI: 10.11159/iccefa24.142

Numerical Analysis of Tunnel Supports in Weak Ground Conditions and High Stress Levels

Giulio Antonucci[1], Gianluca Bella[2-3], Gennaro Scognamiglio[1]
[1]Freelance, Genova, Italy
[2]Pini Group SA, Lugano, Switzerland
[3]University of Applied Sciences and Arts of Southern Switzerland (SUPSI), Mendrisio, Switzerland
ing.antonuccigiulio@libero.it; gianluca.bella@pini.group; ing_scognamiglio@libero.it;

Abstract **-** The reduction of goods and people's travel time is one of the key aspects of the economic development of a country. This goal can be obtained by tunneling, often at great depths, allowing the minimization of the road alignment length. At such depths, the stress state of weak rock masses could lead to high convergence during the excavation works. These high deformations around the tunnel are often incompatible with the standard rock support performance. The current research is intended to preliminary evaluate and compare the performance resulting from the adoption of different rock supports when squeezing occurrence is expected. Finite elements (FE) analyses are carried out to study the stress-strain behavior of a deep circular tunnel excavated into weak rock masses. Several fracturing conditions are considered by taking into account a wide GSI range, while different poor-quality rock mass types are investigated with variations of m_i Hoek & Brown parameters and uniaxial compressive strength. The safety level resulting from the adoption of stiff or sliding ribs is compared in terms of strain and stresses acting on the rock support itself.

Keywords**:** tunneling, deep tunnel, squeezing, weak rock mass.

1. Introduction

Extreme ground response in high-stress, weak rock masses can be encountered in a wide range of deep tunneling projects both mining and civil fields. Indeed, the squeezing behavior of rock masses represents a complex challenge in geotechnical engineering since large deformations can occur around the tunnel over time. The choice of the most appropriate support system is a key aspect when squeezing behavior is expected because it requires careful evaluations of the rock mass stress conditions and its fracturing state, the size and geometry of the underground excavation, the most suitable type, and the required performance of support systems. Therefore, a detailed design with specific construction measures should be taken into account. Many squeezing occurrences during the excavation of deep tunnels are well documented, among them the well-described case of the Saint Martin La Porte access adit (Fig.1a, [1]). There are two basic technical options for accommodating large deformation due to squeezing conditions without damage to the lining as shown in Fig.1b: arranging a compressible layer between the extrados of a stiff lining and the excavation boundary (Fig.1b-I), or installation of a yielding lining in contact with the rock face (Fig.1b-II).

a)

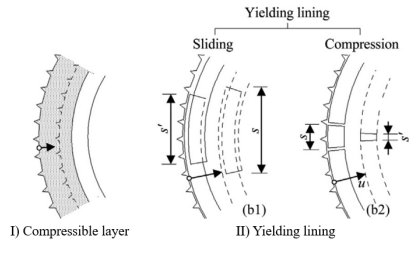

b)

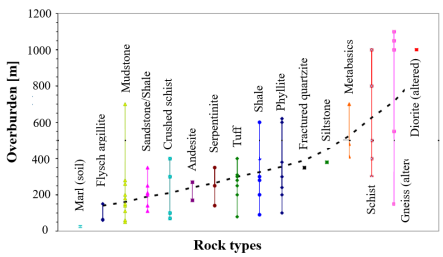

c)

Fig. 1: a) Squeezing at S. Martin la Porte ([1]); b) basic types of flexible support ([2]); c) relations between the various rock types and the overburden in tunnel squeezing cases (modified from [3]).

In the first case is particularly suitable in cases with slow deformations over a long time during the service period of the tunnel. In the second solution, the lining deforms with the rock mass and its circumference decreases. Steel sets with sliding connections can be adopted (Fig.1b-II-b1) or deformable elements installed into slots left between stiff lining segments (Fig.1b-II-b2). Thrust transfer occurs via friction in the case of compressible layers and via compression in the case of yielding elements. More details can be found in [2], [4] and [5].

Within this framework, the current study investigates the safety level and performance of stiff or sliding rock support under squeezing condition are expected when dealing with deep tunnel under high state of stress. Different fracturing state ('Analysis 1'), and different poor-quality rock masses ('Analysis 2') leading to squeezing conditions are considered. The safety level resulting from the adoption of stiff or sliding ribs is studied and compared in terms of strain and stresses acting on the rock supports.

2. Finite Element Analysis

2.1. General concepts

A circular deep tunnel (overburden 600m, radius 5.0m) has been modeled by using the Finite Element Code RS2v.9.0 (RocScience). A constant state of stress and plane strain conditions are assumed (Fig.3), while the model sizes were set to minimize side effects (Fig.2). The rock mass considered for 'Analysis 1' basically consists of Shists (MR=250-1100, average value of MR=550), while in according to fig.1c considering an overburden of 600m for the 'Analysis 2' were analyzed the following rock types: Shale, Phyllite, Metabasics, Schists, Gneiss, and Diorite altered (MR=150 - 1100). Knowledge of the uniaxial compressive strength of the intact rock and MR allowing to estimate the elastic modulus of the intact rock, and therefore the deformability modulus depending on the GSI and disturbance factor D. For the identification and quantification of the squeezing behavior knowledge of the rock mass uniaxial compressive strength σ_{cm} is essential. In this case, it was estimated based on Eqs. (1) proposed by [8] depending on the m_i Hoek-Brown parameter, σ_{ci} uniaxial compressive strength of intact rock, and GSI.

$$\sigma_{cm} = \left(0.0034\, m_i^{0.8}\right) \sigma_{ci}\, [1.029 + 0.025\, e^{(-0.1 m_i)}]^{GSI} \quad (1)$$

The rock mass has been modeled by an elastic-perfectly plastic Hoek-Brown. A wide range of GSI 25-45 (analysis A → analysis E) was adopted in 'Analysis 1' to simulate different fracturing conditions. To reproduce the effects of different poor-quality rock masses were considered a variable range of m_i 8-20 and UCS 10-15MPa (analysis A → analysis I) in 'Analysis 2'. In these conditions "extreme and very severe squeezing problems" are expected (Fig. 2). Unit weight (γ), geological strength index (GSI), Hoek & Brown -m_i parameter (intact rock), uniaxial compressive strength (UCS), Poisson's ratio (v), deformability modulus (E_d), rock mass strength (σ_{cm}), state of stress (p_0), earth pressure coefficient at rest (k_0) are provided in Table 1 and Table 2 for 'Analysis 1' and 'Analysis 2', respectively. Dry conditions were assumed, graded triangular meshes were densified close to the relevant clusters, and tunnel excavation was simulated step-by-step. Rock support (primary lining) has been modeled as a 'standard beam' (Tab.3). The equivalent section per linear meter comprises a 0.20m thick shotcrete layer and double IPN160 ribs spacing 1.5m. Four circumferential sliding slots (each one 0.10m long) are considered to simulate the presence of sliding ribs in the model with deformable lining, thus allowing a circumferential strain of 1.2%. The final lining is made of a steel-reinforced concrete section (Tab.3). In the following curve is represented the classification of squeezing behavior based on the expected tunnel strain and ratio between rock mass strength and in-situ stress.

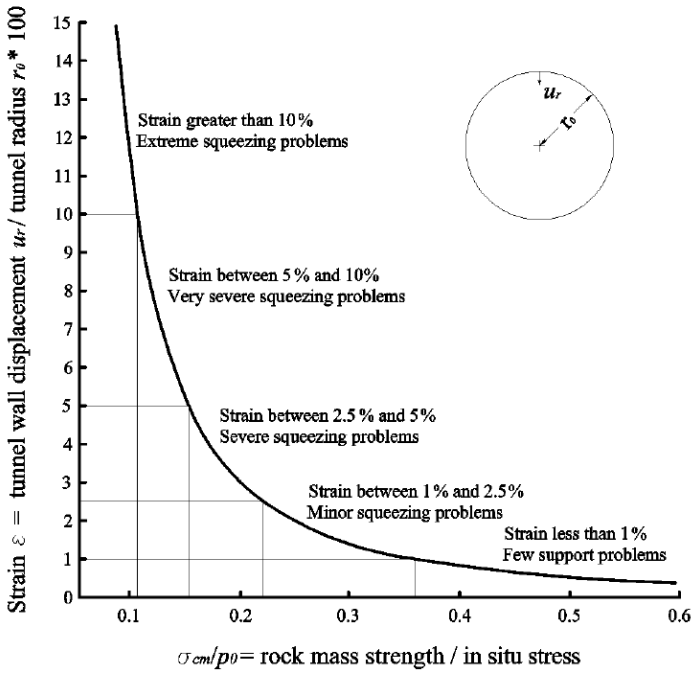

Fig. 2: Classification of squeezing behavior [8].

Table 1: 'Analysis 1'. Rock mass parameters (γ=27kN/m^3, m_i=20, UCS=12MPa, v=0.30, p_0=16.2MPa, k_0=1).

	Analysis A	Analysis B	Analysis C	Analysis D	Analysis E
GSI [-]	25	30	35	40	45
E_d [MPa]	395	537	750	1050	1480
σ_{cm} [MPa]	0.99	1.17	1.37	1.60	1.88
σ_{cm}/p_0 [-]	0.06	0.07	0.08	0.10	0.12
Squeezing problems	Extreme	Extreme	Extreme	Extreme	Very severe

Table 2: 'Analysis 2'. Rock mass parameters of shale, phyllite m_i=8, schists m_i=10, metabasics, gneiss and diorite altered m_i=20 (γ=27kN/m^3, v=0.30, p_0=16.2MPa, k_0=1).

	Analysis A	Analysis B	Analysis C	Analysis D	Analysis E	Analysis F	Analysis G	Analysis H	Analysis I
GSI [-]	40	40	40	40	40	40	40	40	40
m_i [-]	8	10	20	8	10	20	8	10	20
UCS [MPa]	10	10	10	12	12	12	15	15	15
E_d [MPa]	878	878	878	1053	1053	1053	1317	1317	1317
σ_{cm} [MPa]	0.87	0.96	1.34	1.04	1.15	1.60	1.30	1.44	2.00
σ_{cm}/p_0 [-]	0.05	0.06	0.08	0.06	0.07	0.10	0.08	0.09	0.12
Squeezing problems[8]	Extreme	Extreme	Extreme	Extreme	Extreme	Extreme	Extreme	Extreme	Very severe

Table 3: Equivalent rock support and final lining parameters: elastic modulus (E_{eq}), thickness (h_{eq}), area (A_{eq}), inertia (I_{eq}), Poisson's ratio (v), circumferential strain (ε_c), elastic modulus (E), spacing (s), diameter (Φ), rebar depth (d), thickness (h), area (A), inertia (I), compressive strength (σ_c), tensile strength (σ_t).

Rock support (primary lining)										
	E_{eq} [MPa]		h_{eq} [m]		A_{eq} [m^2]		I_{eq} [m^4]	v [-]	ε_c [%]	
Rock support type A: stiff ribs	4435		0.21		0.215		0.000826	0.20	-	
Rock support type B: sliding ribs	4435		0.21		0.215		0.000826	0.20	1.2	
Final lining										
	E [GPa]	s [m]	Φ [mm]	d [mm]	h [m]	A [mm^2/m]	I [m^4]	v [-]	σ_c [MPa]	σ_t [MPa]
Reinforcement (rebar B450C, 2 layers)	200	0.25	16	0.9	-	803 x 2	$8.14 \cdot 10^{-5}$	0.25	450	450
Concrete C20/25	30	-	-	-	1.0	-	-	0.15	25	3

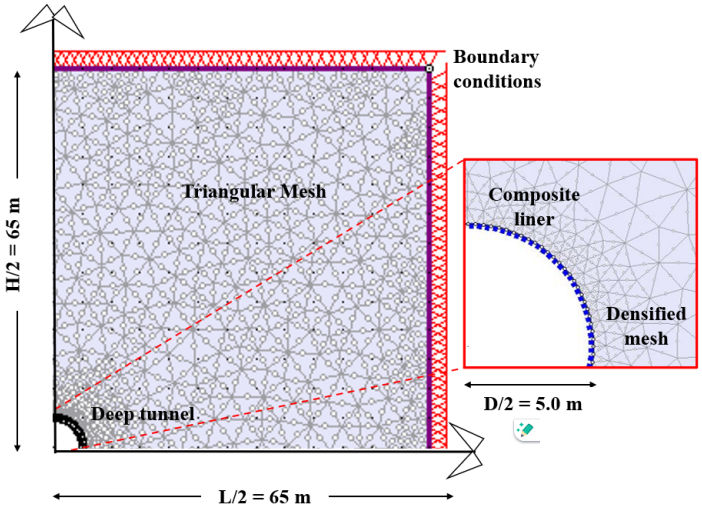

Fig. 3: FE model, geometry, boundary conditions and materials.

Table 4: Finite element model steps and description.

Step.	Description (X=tunnel face distance)
1	in-situ state of stress, p_i/p_0=1.0
2	tunnel face excavation, X=0.0m, p_i/p_0(X)
3	temporary lining installation, X=1.0m, p_i/p_0(X)
4	tunnel excavation advance, X=2.0m, p_i/p_0(X)
5	shotcrete curing at 5 days, X=5.0m, p_i/p_0(X)
6	shotcrete curing at 7 days, X=10.0m, p_i/p_0(X)
7	final lining installation, far from the tunnel face distance, X=20.0m, p_i/p_0=0

2.2. Design approach

Preliminary Convergence-Confinement 2D analysis of the unsupported tunnel is carried out by performing 10 calculation stages (p_i/p_0=1.0, p_i/p_0=0.8, p_i/p_0=0.4, p_i/p_0=0.2, p_i/p_0=0.1, p_i/p_0=0.08, p_i/p_0=0.04, p_i/p_0=0.02, p_i/p_0=0.01 and p_i/p_0=0), so the maximum convergence (u_{max}) and the plastic radius (R_P) of the unsupported tunnel at the final step are obtained. Therefore, the tunnel convergence (u_r) at the relevant distances from the tunnel face (i.e. tunnel face: X=0m; installation of the rock support: X=1m) was then obtained by applying the approach proposed by [6] by knowledge of the ratio R_P/R_T. Radial displacements above estimated allowed for obtaining the ratio p_i/p_0=(1-λ) at the tunnel face and the rock support installation, and so the relaxing factor λ(X) according to the convergence-confinement method ([7]). Finally, the relaxing factors allowed to perform a second series of FE analyses made of two models (Tab.4) to compare the two different rock supports.

3. Results

3.1. 'Analysis 1': results

Table 5 shows a comparison between results obtained from FE analyses considering stiff ribs (rock support type A) or sliding ribs (rock support type B). Figure 4a(top) gives the state of stress MN acting on the rock support type A (red symbols: stiff ribs) and type B (green symbols: deformable ribs) depending on the rock mass fracturing, in terms of the interaction diagram. The safety level is also estimated, as represented in Figure 4a(bottom). Because of the higher radial displacement allowed by deformable ribs, they will result in less stress than stiff ribs. Moreover, the rock mass fracturing does not significantly affect the safety level. These suggest that, within the loading conditions, tunnel shape, and state of stress under investigation, deformable ribs guarantee a higher safety level than rock support type A.

Radial displacement increases when rock mass quality decreases in both cases, sliding or stiff rock support respectively, as shown in Fig.4b. A relevant decrease of radial displacement with rock quality increase can observed in the case of sliding ribs than stiff ribs. Higher differences when stiff or sliding ribs are adopted can be appreciated for GSI between 25-35 (very-poor rock mass quality), but in the case of poor-medium rock mass, non-relevant differences can be noticed.

Table 5: Comparison between stiff and sliding ribs, maximum convergence at final lining installation (u), plastic radius (R_P), axial force (N_{max}), and bending moment (M_{max}).

Analysis			Rock support type A: stiff ribs				Rock support type B: sliding ribs			
	E_d [MPa]	GSI [-]	u [mm]	R_P [m]	N_{max} [MN]	M_{max} [MNm]	u(X=2D) [mm]	R_P [m]	N_{max} [MN]	M_{max} [MNm]
A	395	25	0.53	10.50	12.10	5.00	1.13	15.00	2.94	20.00
B	537	30	0.39	10.10	9.80	3.50	0.68	13.20	3.30	16.00
C	750	35	0.25	9.90	9.31	3.40	0.41	11.70	3.20	12.00
D	1050	40	0.16	8.60	9.20	3.20	0.25	10.40	3.10	9.00
E	1480	45	0.11	8.00	8.30	3.00	0.16	9.90	2.95	7.00

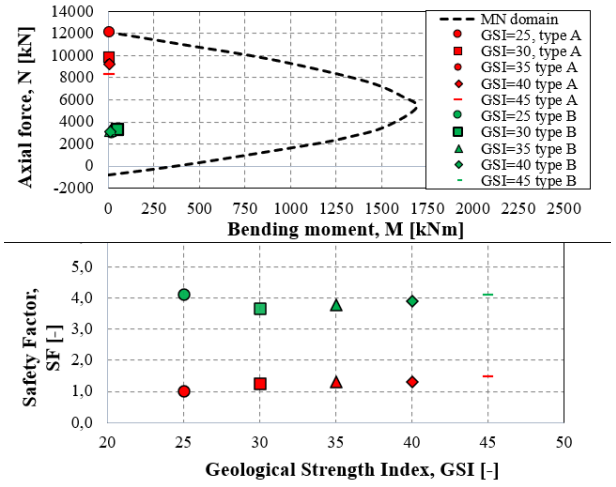

(a)

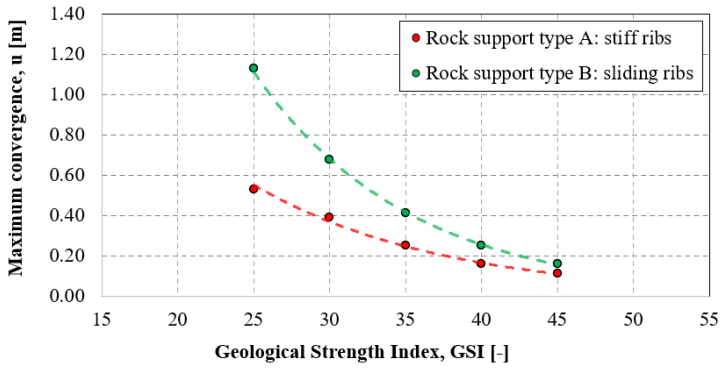

(b)

Fig. 4: Comparison between stiff and sliding ribs. a) Top: MN diagram, bottom: safety factor with GSI; b) maximum convergences when stiff or sliding ribs are installed.

3.2. 'Analysis 2': results

Table 6 summarizes the comparison between numerical results obtained from 'Analysis 2' considering rock support type A (stiff ribs) or type B (sliding ribs) in terms of maximum convergence at final lining installation (u), plastic radius (R_P), characteristic values of the maximum axial force (N_{max}) and maximum bending moment (M_{max}). Numerical outputs are also provided concerning analyses performed considering GSI=40, UCS=12MPa, m_i=10, as shown in Fig. 5-8.

Table 6: Comparison between stiff and sliding ribs in terms of maximum convergence at final lining installation (u), plastic radius (R_P), maximum axial force (N_{max}), maximum bending moment (M_{max}).

Analysis				Rock support type A: stiff ribs				Rock support type B: sliding ribs			
	UCS [MPa]	m_i [-]	E_d [MPa]	u [mm]	R_P [m]	N_{max} [MN]	M_{max} [MNm]	u(X=2D) [mm]	R_P [m]	N_{max} [MN]	M_{max} [MNm]
A	10	8	878	0.34	14.00	14.10	4.00	0.94	22.00	3.40	12.00
B		10		0.30	12.00	12.80	5.00	0.71	17.80	3.40	13.00
C		20		0.21	9.70	9.40	5.00	0.35	11.50	3.20	27.00
D	12	8	1053	0.25	12.50	13.60	5.00	0.63	19.00	3.40	10.00
E		10		0.24	11.60	11.50	5.00	0.49	16.00	3.25	10.00
F		20		0.16	8.80	8.90	9.00	0.25	10.60	3.10	28.00
G	15	8	1317	0.19	11.60	11.15	5.00	0.39	15.50	3.30	10.00
H		10		0.16	10.40	11.00	5.00	0.31	14.20	3.30	15.00
I		20		0.12	8.40	8.00	6.00	0.17	9.80	3.00	30.00

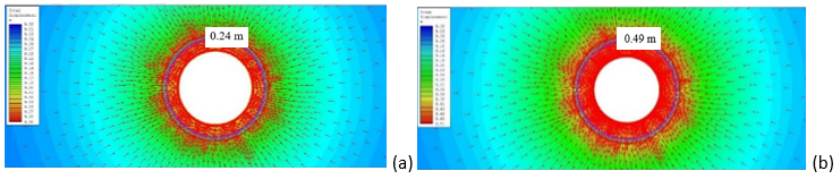

Fig. 5: Analysis n. 5 (UCS=12 MPa – m_i=10) – maximum tunnel convergence in case of stiff ribs (a), and sliding ribs (b)

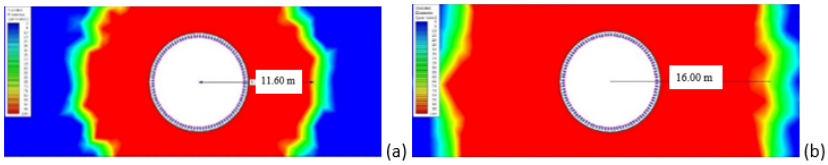

Fig. 6: Analysis n. 5 (UCS=12 MPa – m_i=10) – plastic radius in case of stiff ribs (a), and sliding ribs (b)

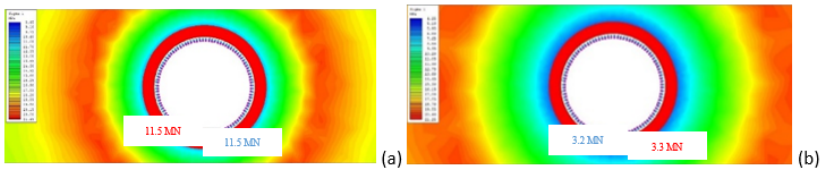

Fig. 7: Analysis n. 5 (UCS=12 MPa – m_i=10) – axial force on the stiff ribs (a), and sliding ribs (b)

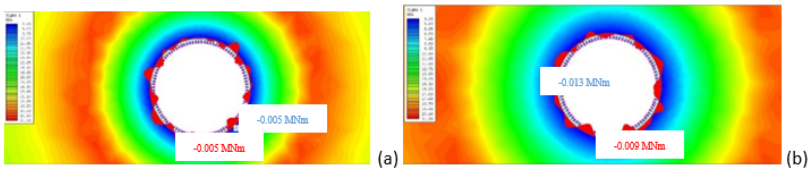

Fig. 8: Analysis n. 5 (UCS=12 MPa – m_i=10) – axial force on the stiff ribs (a), and sliding ribs (b)

In the following figures, the effects caused by UCS and m_i H-B parameter variation in terms of MN domain and safety factor of support are given. The state of stress acting on the rock support type A (red symbols: stiff ribs) and type B (green

symbols: deformable ribs) is shown in Fig.9a and Fig.9b, respectively. The isotropic stress state, the model symmetry, and the circular shape of the tunnel led to obtaining low bending moments compared to the axial forces acting on the rock supports. As shown in Fig.9c, the different poor-quality rock masses reproduced by variation of m_i and UCS, do not significantly affect the safety factor in the case of sliding ribs (type B, green symbols), while for the stiff ribs (type A, red symbols) approximately 40% increase in the safety level can be observed. In the case of deformable ribs, the stress state is less than that of stiff ribs because of the higher convergences allowed by the yielding system. For this reason, under the hypothesis considered in this paper, rock support type B guarantees a higher safety level than stiff ribs when squeezing behavior is expected.

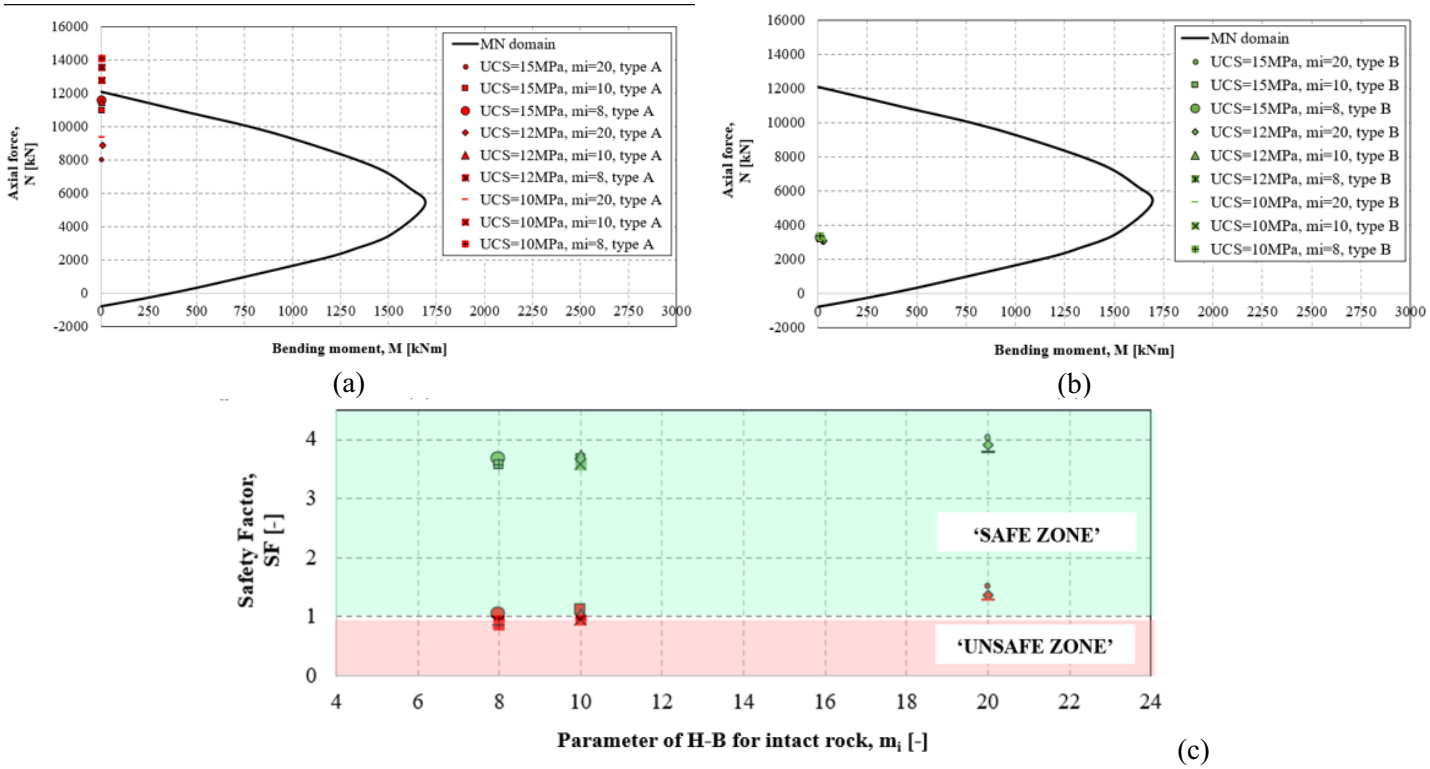

Fig. 9: Interaction MN diagram in case of a) stiff ribs, b) sliding ribs; c) safety factor with m_i and UCS.

The maximum convergences in the case of rock support type A and type B are shown in Fig.10a and Fig.10b, relying on the variation of UCS and m_i.

In the case of very weak-poor quality rock mass (i.e. UCS=10MPa and m_i=8-15) significant convergences between 0.34-0.25m (stiff ribs), or 0.90-0.50m (sliding ribs) can be observed. When dealing with poor-medium rock mass (i.e. UCS=12-15MPa and m_i=15-20), non-relevant differences can be appreciated in terms of convergence. Radial displacement decreases when rock mass quality increases (UCS=10MPa→15MPa, m_i=8→20), in particular higher decrease of convergences is observed in the case of sliding ribs (about 2.5 times) than in stiff ribs (1.5 times) in the condition of constant UCS and variable m_i.

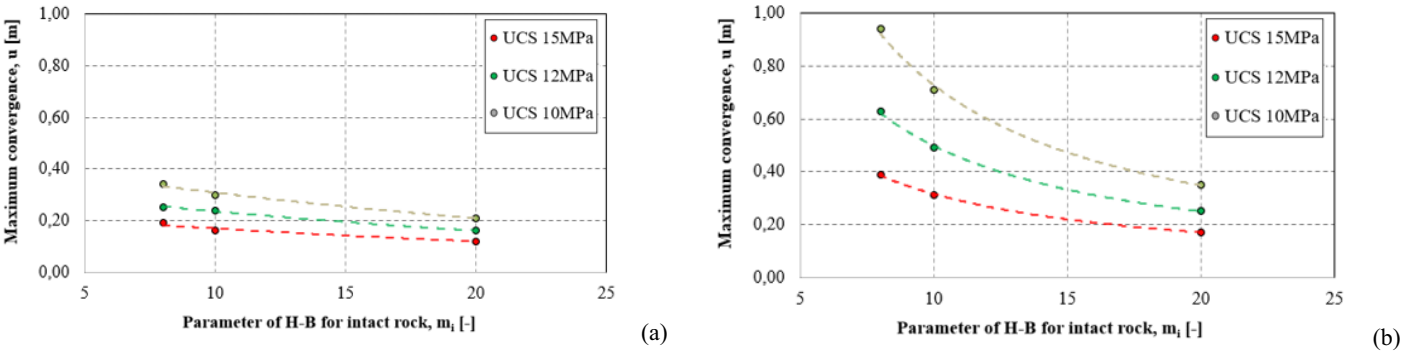

Fig. 10: Maximum convergences when a) stiff ribs, or b) sliding ribs are applied.

4. Conclusion

A preliminary insight is presented on the stress-strain behavior of a deep, circular tunnel excavated into a weak rock mass. The safety level of different types of rock support and rock mass properties is also discussed based on FE calculations thus allowing some considerations when using yielding or stiff rock supports in case of squeezing behavior. Under the assumption assumed in this investigation, 'Analysis 1' suggests that rock mass fracturing does not significantly affect the safety level, while deformable supports guarantee a higher safety level than stiff ones.

Moreover, 'Analysis 2' suggests that the yielding support is more sensitive in the case of weak-poor quality rock mass because the sliding elements allow higher convergences and lower stress state than stiff supports, so obtaining a higher safety factor. In the case of stiff ribs, the safety check is not satisfied when dealing with weak-poor quality rock types. On the other hand, for medium-quality rock types, when both stiff ribs or sliding ribs are applied, the safety factor is guarantee and its increase significantly with the improvement of geomechanical parameters.

References

[1] G. Barla, "Innovative tunneling construction method to cope with squeezing at the Saint Martin La Porte access adit (Lyon-Turin Base Tunnel)", in *Proceedings of the Eurock 2009 Rock Engineering in Difficult Ground Conditions*, Dubrovnik, Croatia, 2009, vol. 1, pp. 1-10.

[2] M. Ghorbani, K. Shahriar, M. Sharifzadeh, R. Masoudi, "A critical review on the developments of rock support systems in high stress ground conditions", *International Journal of Mining Science and Technology*, vol. 30, pp. 555-572, 2020.

[3] G.L. Shrestha, "Stress induced problems in Himalayan tunnels with special reference to squeezing", Doctoral Thesis, Norwegian University of Science and Technology, Trondheim, 2005.

[4] R. Das, "Tunnelling in squeezing ground – a review on prediction and measurement of boundary deformation and available mitigation methods", in *Proceedings of the Conference: 5th International Disaster Risk and Vulnerability Conference (DRVC 2023)*, Kerala, India, 2023.

[5] N. Radoncic, W. Schubert and B. Moritz "Ductile support design", *Geomechanics and Tunnelling*, vol. 2, no.5, 2009.

[6] N. Vlachopoulos and M.S. Diederichs, "Improved longitudinal displacement profiles for convergence confinement analysis of deep tunnels", *Rock Mechanics and Rock Engineering*, vol. 42, no.2, pp. 131-146, 2009.

[7] M. Panet and A. Guenot, "Analysis of convergence behind the face of a tunnel", in *Proceeding of the International Symposium Tunnelling, (IST'82)*, The Institution of Mining and Metallurgy, London, pp. 197-204, 1982.

[8] E. Hoek and P. Marinos "Predicting tunnel squeezing problems in weak heterogeneous rock masses", *Tunnels and Tunnelling International,* Part 1 – Part 2, 2000.